Sparsity-based Time-Frequency Analysis for Automatic Radar Waveform Recognition

Shuimei Zhang, Ammar Ahmed, and Yimin D. Zhang
Department of Electrical and Computer Engineering
Temple University, Philadelphia, PA 19122, USA

***Abstract*—In this paper, we develop a novel pre-processing algorithm to achieve effective signal denoising for improved recognition of noisy radar signals. The algorithm is considered in the instantaneous autocorrelation function domain in which time or lag slices are converted to a Hankel matrix, and an atomic norm-based method is applied to mitigate the impacts of noise. Cross-terms are suppressed by using a time-frequency kernel, such as the Choi-Williams distribution, and a sparsity-based reconstruction technique is utilized to obtain a high-resolution time-frequency distribution of the radar waveforms. Simulation results verify the effectiveness of the proposed method. The proposed denoising algorithm for radar waveform recognition enables a substantial increase of the overall successful recognition rate from 90.24% to 97.76%.**

***Index Terms*—Radar waveform recognition, non-stationary signal, time-frequency analysis, sparse reconstruction, atomic norm.**

I. Introduction

Automatic radar waveform recognition plays an important role in electronic warfare, such as radar emitter identification and threat detection. This becomes even more critical when radars adopt low probability of intercept (LPI) radar waveforms that differ to the traditional linear frequency modulated (LFM) waveforms for pulse compression [1]. Commonly used LPI radar waveforms include those based on nonlinear frequency modulation (FM) and polyphase code modulation [2]. Examples of polyphase codes include the Frank, P1, P2, P3, and P4 codes [3], [4]. The objective of radar waveform recognition is to detect and classify the received radar signals based on the pulse compression waveform [5].

A number of methods have been proposed to recognize radar signals with different kinds of modulations. Feature extraction and classifier design are two key procedures for radar waveform recognition [6]. Selection of an effective feature extraction algorithm is important to achieve a desirable waveform classification performance. Because of the sparsity of many non-stationary signals, including the above mentioned LPI radar waveform signals, in the time-frequency (TF) domain, this domain is effective for signal characterization and feature extraction. The objective of this paper is to provide an enhanced TF representation (TFR) of noisy LPI radar signals to enable improved feature extraction.

The ability to recognize the time-varying frequency variations enables classification of different modulations [6]. In order to achieve this, bilinear TF analysis is widely adopted for radar waveform recognition due to its high energy concentration. The Wigner-Ville distribution (WVD) is commonly referred to as the prototype bilinear TF distribution. However, the bilinear nature of the WVD renders cross-terms to appear midway between true signal components in the case of nonlinear or multi-component signals. Such cross-terms prohibit accurate analysis and interpretation of the signal instantaneous frequency (IF) signatures [7]–[10]. In this case, TF kernels are used to mitigate the effects of cross-terms so as to readily determine the modulation type and estimate the modulation parameters. Among the many available TF kernels, the Choi-Williams distribution (CWD), which is based on exponential weighting in both time and lag domains, is considered as a favorable choice because of its simplicity and robustness to different signal parameters [5], [6], [11].

Existing methods reported in the open literature, however, do not provide a high-resolution TFR and render poor TFR when the LPI radar signals are noisy. There are limited works reporting signal denoising. In [6], the authors applied a designed filter to smooth the TFR, where each point on the TFR is updated by averaging the points within the coverage of a square. In [12], image morphology algorithm was utilized for noise removing after converting the TFR into a binary image. In [3], signal denoising was achieved by a nonlinear wavelet transformation technique. However, the denoising capability of these methods are limited.

In this paper, we propose a novel pre-processing algorithm for feature enhancement of noisy radar waveforms. The algorithm is considered in the instantaneous autocorrelation function (IAF) domain, which is related to the TFR by a one-dimensional (1-D) Fourier transform with respect to lag for each time slice or the ambiguity function (AF) with respect to time for each lag slice. In the IAF domain, each time- or lag-domain slice is converted to a Hankel matrix to denoise the IAF entries via the atomic norm-based approach. Then, CWD is utilized to mitigate the cross-terms and further reduce the residual effect of noise. Finally, sparse TFR reconstruction techniques are used to further improve the sparsity of the yielding TF estimate. To our best knowledge, the sparsity of the FM and polyphase code LPI radar signals in the TF domain has not been considered for radar waveform recognition. The proposed method can be easily of joint use with any other pre-processing techniques.

Notations: Lower-case (upper-case) bold characters are used to denote vectors (matrices). $(\cdot)^*$, $(\cdot)^{\mathrm{T}}$ and $(\cdot)^{\mathrm{H}}$ denote the complex conjugation, transpose and the Hermitian trans-

pose, respectively. $\mathcal{F}_x(\cdot)$ and $\mathcal{F}_x^{-1}(\cdot)$ represent the discrete Fourier transform (DFT) and inverse DFT (IDFT) with respect to x, respectively. $\boldsymbol{Y} = \mathcal{H}(\boldsymbol{x}, p)$ converts vector $\boldsymbol{x}$ to Hankel matrix $\boldsymbol{Y}$ with pencil parameter p, whereas $\boldsymbol{x} = \hbar(\boldsymbol{Y})$ defines the inverse operation of Hankel matrix conversion. $\lceil\cdot\rceil$ denotes the ceiling function.

II. Signal Model and Time-Frequency Representation

A. Signal Model

Consider a discrete-time signal, $x(t), t = 1, ..., T$,

$$x(t) = s(t) + n(t) = a(t)e^{\jmath\psi(t)} + n(t), \tag{1}$$

where $\jmath = \sqrt{(-1)}$ is the imaginary unit, $s(t)$ is the transmitted signal with the phase law $\psi(t)$, and $n(t)$ is the additive white Gaussian noise.

The instantaneous frequency of $x(t)$ is expressed as:

$$f(t) = \frac{1}{2\pi}\frac{\mathrm{d}\psi(t)}{\mathrm{d}t}. \tag{2}$$

B. Instantaneous Auto-correlation Function

The IAF of the transmitted signal $s(t)$ and the received signal $x(t)$ are respectively defined as

$$R_{ss}(t,\tau) = s\left(t+\frac{\tau}{2}\right)s^*\left(t-\frac{\tau}{2}\right), \tag{3}$$

and

$$R_{xx}(t,\tau) = x\left(t+\frac{\tau}{2}\right)x^*\left(t-\frac{\tau}{2}\right), \tag{4}$$

where τ is the time lag. Denote vector $\boldsymbol{y}^t$ as an IAF slice of the transmitted signal $s(t)$ that contains all IAF entries along the τ dimension corresponding to time t. The IAF slice $\boldsymbol{y}^t$ is Hermitian symmetric about $\tau_I = 0$, where I is the index of the center element in $\boldsymbol{\tau}$. In other words, $\boldsymbol{y}^t$ has the following property:

$$\left[y^t_{I-1}, \cdots, y^t_2, y^t_1\right]^{\mathrm{H}} = \left[y^t_{I+1}, \cdots, y^t_{Q-1}, y^t_Q\right]^{\mathrm{T}}, \tag{5}$$

where $\boldsymbol{\tau} = [\tau_1, \cdots, \tau_Q]^{\mathrm{T}}$ denotes the lag vector, and Q is the cardinality of $\boldsymbol{\tau}$.

We similarly define $\boldsymbol{z}^t$ as the IAF slice of the received signal $x(t)$ along the τ dimension. Then, $\boldsymbol{z}^t$ is also Hermitian symmetric, i.e.,

$$\left[z^t_{I-1}, \cdots, z^t_2, z^t_1\right]^{\mathrm{H}} = \left[z^t_{I+1}, \cdots, z^t_{Q-1}, z^t_Q\right]^{\mathrm{T}}. \tag{6}$$

C. Wigner-Ville Distribution

The DFT of the IAF $R_{xx}(t,\tau)$ with respect to τ is the well-known WVD, i.e.,

$$W_{xx}(t,f) = \mathcal{F}_\tau[R_{xx}(t,\tau)] = \int_\tau R_{xx}(t,\tau)e^{-\jmath 2\pi f\tau}d\tau. \tag{7}$$

Because $R_{xx}(t,\tau)$ is Hermitian symmetric, the WVD of the observed data is real-valued.

D. Ambiguity Function

The AF is obtained by applying 1-D DFT to the IAF $R_{xx}(t,\tau)$ with respect to t, expressed as

$$A_{xx}(\theta,\tau) = \mathcal{F}_t[R_{xx}(t,\tau)] = \int_t R_{xx}(t,\tau)e^{-\jmath 2\pi\theta t}dt, \tag{8}$$

where θ is the frequency shift, also known as Doppler. Note that, unlike WVD, the AF entries are in general complex since the IAF is Hermitian symmetric only with respect to τ but not with respect to t.

III. Proposed Method

A. Signal Denoising via Atomic Norm

At time instant t, we assume P frequency components are present, i.e., there exist P nonzero entries in the TFR corressponding to the specific value of t. From (7), we know that the IAF is the 1-D IDFT of the WVD with respect to frequency f. Therefore, the IAF slice $\boldsymbol{y}^t$ at time instant t can be expressed as

$$\boldsymbol{y}^t = \mathcal{F}_f^{-1}(\boldsymbol{w}^t) = \sum_{p=1}^{P} c_p e^{\jmath 2\pi f_p \boldsymbol{\tau}}, \tag{9}$$

where c_p denotes the complex amplitude of the p-th signal component, f_p is the corresponding signal frequency, and $\boldsymbol{w}_t$ denotes the TF slice along the f dimension at time instant t.

We solve this signal denoising problem in the context of Hankel matrix completion [13], [14] by forming the following Hankel matrix from $\boldsymbol{y}^t$:

$$\boldsymbol{H}^t_y = \mathcal{H}(\boldsymbol{y}^t, q_1) = \begin{bmatrix} y^t_1 & y^t_2 & \cdots & y^t_{q_2} \\ y^t_2 & y^t_3 & \cdots & y^t_{q_2+1} \\ \vdots & \vdots & \ddots & \vdots \\ y^t_{q_1} & y^t_{q_1+1} & \cdots & y^t_Q \end{bmatrix}, \tag{10}$$

where q_1 is the pencil parameter, which is usually set to $\lceil Q/2\rceil$, and $q_2 = Q - q_1 + 1$.

The same P frequency components are shared among all the columns in $\boldsymbol{H}^t_y$. The atom set for $\boldsymbol{H}^t_y$ can be expressed as

$$\mathcal{A} = \{\boldsymbol{A}(f,\boldsymbol{\phi}) | f \in [0,1), \|\boldsymbol{\phi}\|_2 = 1\}, \tag{11}$$

where $\boldsymbol{A}(f,\boldsymbol{\phi})$ is an atom representing $\boldsymbol{H}^t_y$ and is formulated as

$$\boldsymbol{A}(f,\boldsymbol{\phi}) = \boldsymbol{a}(f)\boldsymbol{\phi}^{\mathrm{H}}, \tag{12}$$

$\boldsymbol{a}(f) = e^{\jmath 2\pi f\boldsymbol{\tau}} \in \mathbb{C}^{q_1}$, $f \in [0,1)$, $\boldsymbol{\phi} \in \mathbb{C}^{q_2}$ with $\|\boldsymbol{\phi}\|_2 = 1$. Note that atomic norm approach avoids the off-grid issue by exploiting the continuity of the frequency set.

The atomic norm of $\boldsymbol{H}^t_y$ can be obtained by solving the following problem [15]–[17]:

$$\begin{aligned}\|\boldsymbol{H}^t_y\|_{\mathcal{A}} &= \inf\left\{\beta > 0 : \boldsymbol{H}^t_y \in \beta\mathrm{conv}(\mathcal{A})\right\} \\ &= \inf\left\{\sum_p |c_p| : \boldsymbol{H}^t_y = \sum_p |c_p|\boldsymbol{a}(f_p,\boldsymbol{\phi}_p)\right\},\end{aligned} \tag{13}$$

where $\mathrm{conv}(\mathcal{A})$ is the convex hull of $\mathcal{A}$.

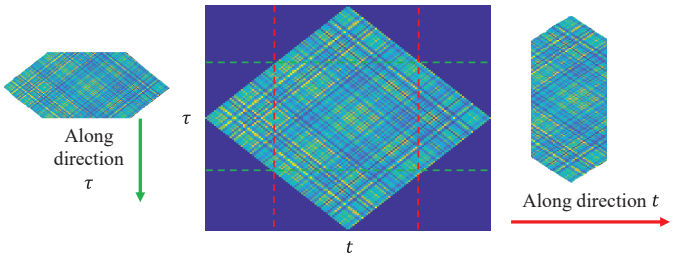

Fig. 1. The noisy IAF for atomic norm-based processing.

Define $\boldsymbol{H}_z^t = \mathcal{H}(\boldsymbol{z}^t, q_1)$ as the Hankle matrix obtained from the noisy IAF slice at time instant t, the signal denoising problem can be expressed as

$$\hat{\boldsymbol{H}}_y^t = \arg\min_{\boldsymbol{H}_y^t} \frac{1}{2}\|\boldsymbol{H}_z^t - \boldsymbol{H}_y^t\|_F^2 + \eta\|\boldsymbol{H}_y^t\|_{\mathcal{A}}, \tag{14}$$

where η is a regularization parameter trading off between the fidelity of the Hankel matrix fitting and the atomic norm. Problem (14) can be reformulated as

$$\begin{aligned} \min_{\boldsymbol{H}_y^t, \boldsymbol{u}, \boldsymbol{W}} \quad & \frac{1}{2}\|\boldsymbol{H}_z^t - \boldsymbol{H}_y^t\|_F^2 + \frac{\eta}{2}(\mathrm{Tr}(\mathcal{T}(\boldsymbol{u})) + \mathrm{Tr}(\boldsymbol{W})) \\ \text{s.t.} \quad & \begin{bmatrix} \mathcal{T}(\boldsymbol{u}) & \boldsymbol{H}_y^t \\ (\boldsymbol{H}_y^t)^{\mathrm{H}} & \boldsymbol{W} \end{bmatrix} \succeq 0, \end{aligned} \tag{15}$$

where $\mathrm{Tr}(\cdot)$ denotes the trace operator and $\mathcal{T}(\boldsymbol{u})$ denotes a Hermitian Toeplitz matrix with $\boldsymbol{u}$ as its first column. Problem (15) can be effectively solved via the alternating direction method of multipliers (ADMM) approach [18] as outlined in [19]. Based on the obtained $\hat{\boldsymbol{H}}_y^t$, we can estimate the denoised IAF slice as

$$\hat{\boldsymbol{y}}^t = \hbar(\hat{\boldsymbol{H}}_y^t). \tag{16}$$

For the underlying problem, the Hermitian symmetry property of the IAF can be used to reduce the computational complexity. For each time instant t, $\hat{\boldsymbol{y}}^t$ have a Hermitian symmetric structure, given as

$$\hat{\boldsymbol{y}}^t = \left[\hat{y}_1^t, \cdots, \hat{y}_{I-1}^t, \hat{y}_I^t, \left(\hat{y}_{I-1}^t\right)^*, \cdots, \left(\hat{y}_1^t\right)^*\right]^{\mathrm{T}}. \tag{17}$$

In practice, $x(t)$ is of a finite length, which leads to a diamond shape with a time-varying width of $Q = T - |T + 1 - 2t|$ in the IAF due to zero-padding.

When the signals are processing in batch, the denoising procedure becomes unreliable when Q is small because of zero-padding. To avoid this issue, we denoise the entries of $\boldsymbol{z}^t$ by utilizing both time and lag slices as proposed in [14]. As shown in Fig. 1, the area for $0.25T \le t \le 0.75T$ are first recovered by utilizing the time slice along the lag domain as depicted above. The similar 1-D DFT relationship between the IAF and the AF as well as the sparsity of the AF are exploited to denoise the entries for $0 \le \tau \le 0.25T$ by utilizing the lag slices.

B. Choli-Williams Distribution

The analysis and interpretation of the signal IF signatures become cumbersome in the presence of cross-terms as a result of the bilinear WVD. A number of TF kernels are developed to suppress cross-terms while preserving auto-terms. In this paper, we use the CWD, which is defined for a continuous-time signal $x(t)$ as [20]

$$\begin{aligned} W_{CW} = \int_{-\infty}^{\infty}\int_{-\infty}^{\infty} \frac{1}{\sqrt{4\pi\tau^2/\sigma}} \exp\left(-\frac{(t-\mu)^2}{4\tau^2/\sigma}\right) \\ \cdot\, x\left(t+\frac{\tau}{2}\right) x^*\left(t-\frac{\tau}{2}\right) \exp(-j\omega\tau)\mathrm{d}t\mathrm{d}\tau, \end{aligned} \tag{18}$$

where $\sigma > 0$ is a scaling factor that controls the attenuation. The CWD uses an exponential kernel function

$$\Phi(\theta, \tau) = \exp\left(-\theta^2\tau^2/\sigma\right). \tag{19}$$

C. Obtaining TF distribution Using Sparse Reconstruction

FM and polyphase code LPI radar signals are sparsely presented in the TF domain. To perform sparsity-based TFR reconstruction, we utilize the 1-D IDFT relationship between the TF slice $\boldsymbol{w}^t$ and the IAF slice $\boldsymbol{y}^t$ at time instant t, i.e.,

$$\boldsymbol{y}^t = \boldsymbol{G}_f \boldsymbol{w}^t, \quad \forall t, \tag{20}$$

where $\boldsymbol{G}_f$ is a matrix performing the 1-D IDFT with respect to f. As such, the sparse reconstruction problem for (20) is described as

$$\min ||\boldsymbol{w}^t||_1 \quad \text{s.t.} \quad \boldsymbol{y}^t - \boldsymbol{G}_f \boldsymbol{w}^t = 0, \quad \forall t. \tag{21}$$

Many compressive sensing techniques can be used to solve (21), such as the orthogonal matching pursuit (OMP) [21] and Bayesian sparse learning techniques [22], [23]. In this paper, OMP is applied at each time instant because OMP allows us to specify the sparsity at each time instant.

IV. Simulation Results

As an example of the LPI radar waveforms, we consider the P2 code as an example. P2 code waveforms have a stair-wise frequency signature and thus are difficult to be accurately represented in the TF domain as compared to other waveforms whose frequency changes straightly with the time, such as the P3 and P4 code waveforms. Therefore, preserving the stair-wise frequency signature is critical to distinguish the underlying waveform from those whose frequency signature varies linearly with time. The phase of P2 code signal is varied according to [1]:

$$\phi_{i,j} = -\frac{\pi}{2M}[2i - 1 - M][2j - 1 - M], \tag{22}$$

where $i, j = 1, 2, \cdots, M$ and M is the order. In our simulations, the carrier frequency is $1/4$ of the sampling frequency. The cycles per phase code is 1 and the number of phase M is set as 6.

Fig. 2 shows the real-part of the P2 code radar waveform and the corresponding IAF magnitude, WVD, and CWD. No noise is considered in these results. For the single-component signal with a constant amplitude, the IAF has a constant

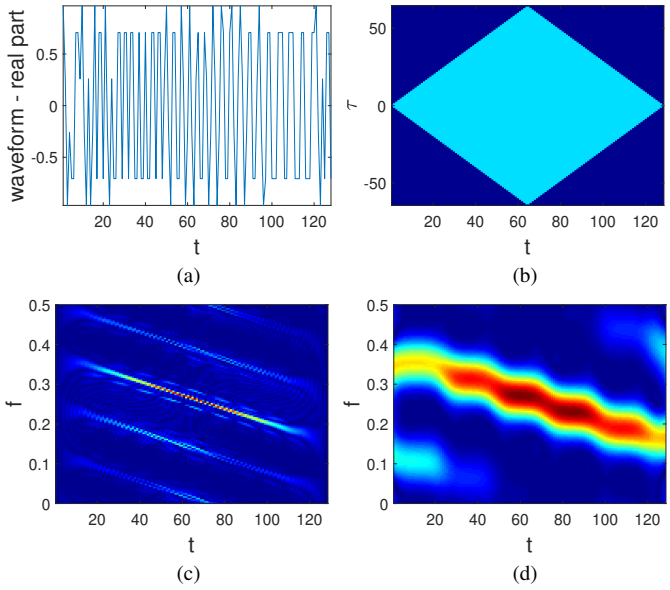

Fig. 2. P2 code signal without the noise. (a) Real-part waveform. (b) IAF. (c) WVD. (d) CWD.

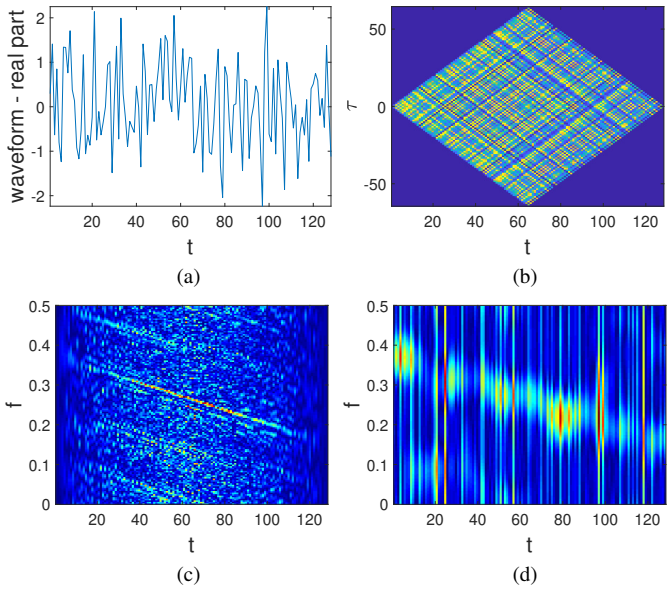

Fig. 3. P2 code signal in the noisy environment (SNR = 0 dB). (a) Real-part waveform. (b) IAF. (c) WVD. (d) CWD.

magnitude within the diamond-shaped region. We observe that the WVD does not provide a clear signal TF signature due to the cross-term effects even though no noise is present. The CWD depicted in Fig. 2(d) shows a clear TF signature, while the TF resolution is poor.

In Fig. 3, we show the results with added noise, where the input signal-to-noise ratio (SNR) is 0 dB. As a result, the waveform magnitude varies randomly, as shown in Fig. 3(a). The IAF becomes noisy and the magnitude does not maintain a constant value. Due to the existence of noise, aliases appear in the WVD compared to Fig. 2(d). On the other hand, the CWD in Fig. 3(c) is distorted heavily by the noise. It is difficult to

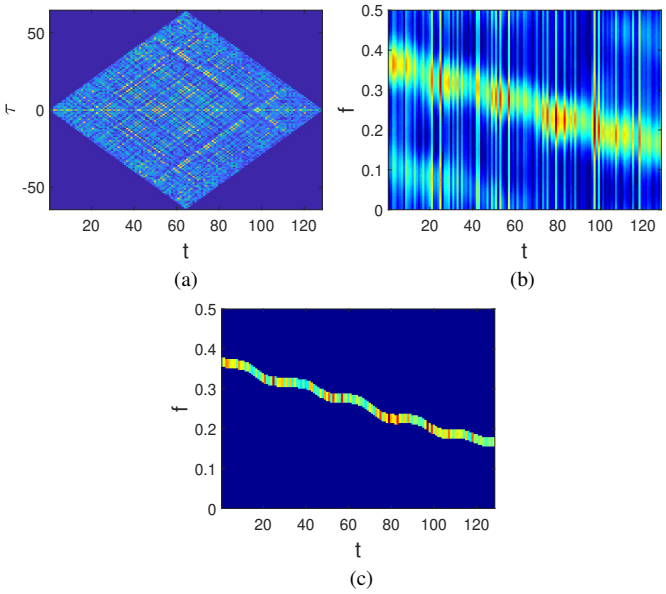

Fig. 4. P2 code signal in the noisy environment (SNR = 0 dB). (a) IAF denoised via atomic norm. (b) denoised CWD. (c) proposed TFR (atomic norm + CWD + OMP).

TABLE I
LIST OF THE PARAMETERS OF SIMULATED SIGNALS

Signal Waveforms	Parameter	Uniform Ranges
	Sampling rate (f_s)	U(1)
P2	Carrier frequency (f_c) Cycles per phase (cpp) Frequency steps (m)	U(1/8, 1/4) [1, 5] [4, 8]
P3, P4	Carrier frequency (f_c) Cycles per phase (cpp) Frequency steps (m)	U(1/8, 1/4) [1, 5] [32, 70]
LFM	Initial frequency (f_0) Bandwidth (Δf)	U(1/16, 1/8) U(1/16, 1/8)
Costas codes	Number change Fundamental frequency (f_{min})	[3, 6] U(1/24, 1/20)

recognize the auto-term TF distributions.

Fig. 4 depicts the performance of the proposed method in the same noisy environment as in Fig. 3. Fig. 4(a) depicts the recovered IAF via the atomic norm-based approach, which performs denoising on the IAF entries. We notice that the recovered IAF has a much smaller number of high values than that in the noisy IAF depicted in Fig. 3(b) and is close to the noise-free IAF as shown in Fig. 2(b). The CWD obtained from the recovered IAF is shown in Fig. 4(b). In comparison to Fig. 3(d), the denoised CWD provides a much more smooth TF signature. Fig. 4(c) shows the final TFR obtained through sparse reconstruction using OMP. It is clear that the proposed method not only mitigates the effects of the noise, but also provides a high-resolution TFR, thereby significantly improving the feature representation of the radar signals.

To verify the effectiveness of the proposed method in wave-

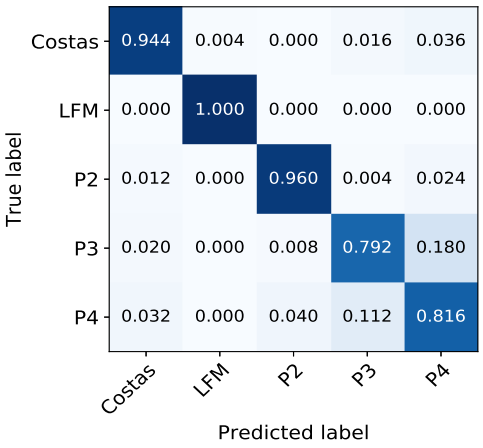

(a)

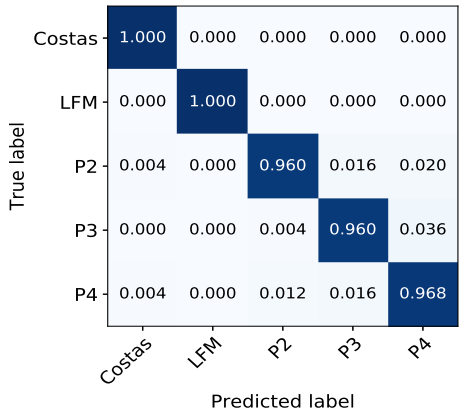

(b)

Fig. 5. Normalized confusion matrix for classification performance comparison. (a) CWD-based TFRs; (b) Proposed TFRs (atomic norm + CWD + OMP)

TABLE II
LIST OF THE PARAMETERS OF THE CNN STRUCTURE

Layer (type)	Parameter Setting
Batch normalization	–
Convolution 1	7 kernels, size 5×5, stride 1
Maximum pooling 1	size 2×2, stride 2
Convolution 2	4 kernels, size 5×5, stride 1
Maximum pooling 2	size 2×2, stride 2
Convolution 3	4 kernels, size 5×5, stride 1
Maximum pooling 3	size 2×2, stride 2
Flatten layer	–
Fully connected layer 1	100 neurons
Fully connected layer 2	5 neurons

form classification, we process the results using a convolution neural network (CNN) [24], [25]. Five types of waveforms, including Costas, LFM, P2, P3 and P4, are considered for classification. The detailed parameter settings are shown in Table I. $\mathrm{U}(\cdot)$ denotes a uniform distribution of the frequency. $1,000$ samples are generated for each waveform class, from which 75% of the samples are utilized for training and the remaining 25% are utilized for testing. The input SNR is set to 0 dB. The size of the input TFR images is 128×128. Two classifiers are trained, one using the traditional CWD results and the other one using the proposed atomic norm-based pre-processing method in the sparse reconstruction framework (atomic norm + CWD + OMP). Both classifiers share the same structure and hyper-parameters, which are depicted in Table II. ReLU is chosen as the activation function for each convolution layer. Keras with Tensorflow backend is adopted for CNN implementation.

The classification results obtained using the two TFRs are shown in Fig. 5. The average accuracy of the testing classification is 90.24% for traditional CWD-based TFRs and 97.76% for the TFRs obtained from the proposed method. In particular, the recognition rate between the challenging pair of P3 and P4 has been greatly improved by the proposed atomic norm-based pre-processed method.

V. CONCLUSION

In this paper, we proposed a novel pre-processing algorithm for the recognition of noisy LPI radar waveforms. We exploit the atomic norm-based denoising operation in instantaneous autocorrelation function domain followed by cross-term suppression using CWD. Sparsity-base reconstruction technique is employed to obtain a high-resolution TF distribution. The effectiveness of the proposed approaches is evidently demonstrated using simulation results processed for the P2 coded radar signal. Furthermore, the classification result using the CNN demonstrates that the proposed method enables an improvement of the overall recognition accuracy from 90.24% to 97.76%.

REFERENCES

[1] P. E. Pace, *Detecting and Classifying Low Probability of Intercept Radar*, 2nd ed. Norwood, MA, USA: Artech House, 2009.

[2] M. I. Skolnik, *Introduction to Radar Systems*, 2nd ed. New York, NY, USA: McGraw-Hill, 1981.

[3] T. R. Kishore and K. D. Rao, "Automatic intrapulse modulation classification of advanced LPI radar waveforms," *IEEE Trans. Aerosp. Electron. Syst.*, vol. 53, no. 2, pp. 901–914, April 2017.

[4] C. Shi, F. Wang, M. Sellathurai, and J. Zhou, "Low probability of intercept-based distributed MIMO radar waveform design against barrage jamming in signal-dependent clutter and coloured noise," *IET Signal Process.*, vol. 13, no. 4, pp. 415–423, May 2019.

[5] J. Lunden and V. Koivunen, "Automatic Radar Waveform Recognition," *IEEE J. Sel. Topics Signal Process.*, vol. 1, no. 1, pp. 124–136, June 2007.

[6] C. Wang, J. Wang, and X. Zhang, "Automatic radar waveform recognition based on time-frequency analysis and convolutional neural network," in *Proc. IEEE Int. Conf. Acoust., Speech Signal Process.,* Mar. 2017, pp. 2437–2441.

[7] B. Boashash (ed.), *Time-Frequency Signal Analysis and Processing: A Comprehensive Reference, 2nd ed.* Academic Press, 2015.

[8] Y. D. Zhang, "Resilient quadratic time-frequency distribution for FM signals with gapped missing data," in *Proc. IEEE Radar Conf.*, Seattle, WA, May 2017, pp. 1765–1769.

[9] V. S. Amin, Y. D. Zhang, and B. Himed, "Improved instantaneous frequency estimation of multi-component FM signals," in *Proc. IEEE Radar Conf.*, Boston, MA, April 2019.

[10] V. S. Amin, Y. D. Zhang, and B. Himed, "Sparsity-based time-frequency representation of FM signals with burst missing samples," *Signal Process.*, vol. 155, pp. 25–43, Feb. 2019.

[11] Q. Guo, X. Yu, and G. Ruan, "LPI radar waveform recognition based on deep convolutional neural network transfer learning," *Symmetry*, vol. 11, no. 4, pp. 540, April 2019.

[12] M. Zhang, M. Diao, L. Gao, and L. Liu "Neural networks for radar waveform recognition," *Symmetry*, vol. 9, no. 5, pp. 75, May 2017.

[13] Y. Chen and Y. Chi, "Harnessing structures in big data via guaranteed low-rank matrix estimation: recent theory and fast algorithms via convex and nonconvex optimization," *IEEE Signal Process. Mag.*, vol. 35, no. 4, pp. 14–31, July 2018.

[14] S. Zhang and Y. D. Zhang, "Robust time-Frequency analysis of multiple FM signals with burst missing samples," *IEEE Signal Process. Lett.*, vol. 26, no. 8, pp. 1172–1176, June 2019.

[15] V. Chandrasekaran, B. Recht, P. A. Parrilo, and A. S. Willsky, "The convex geometry of linear inverse problems," *Found. Comput. Math.*, vol. 12, no. 6, pp. 805–849, Dec. 2012.

[16] G. Tang, B. Bhaskar, P. Shah, and B. Recht, "Compressed sensing off the grid," *IEEE Trans. Inf. Theory*, vol. 59, no. 11, pp. 7465–7490, Nov. 2013.

[17] Z. Yang and L. Xie, "On gridless sparse methods for line spectral estimation from complete and incomplete data," *IEEE Trans. Signal Process.*, vol. 63, no. 12, pp. 3139–3153, June 2015.

[18] S. Boyd, N. Parikh, E. Chu, B. Peleato, and J. Eckstein, "Distributed optimization and statistical learning via the alternating direction method of multipliers," *Found. Trends Mach. Learn.,* vol. 3, no. 1, pp. 1–122, Jan. 2011.

[19] Y. Li and Y. Chi, "Off-the-grid line spectrum denoising and estimation with multiple measurement vectors," *ArXiv Preprint ArXiv:1408.2242*, 2014.

[20] H. I. Choi and W. J. Williams, "Improved time-frequency representation of multicomponent signals using exponential kernels," *IEEE Trans. Acoust., Speech, Signal Process.*, vol. 37, no. 6, pp. 862–871, June 1989.

[21] J. A. Tropp and A. C. Gilbert, "Signal recovery from random measurements via orthogonal matching pursuit," *IEEE Trans. Inf. Theory*, vol. 53, no. 12, pp. 4655-4666, 2007.

[22] S. Ji, Y. Xue, and L. Carin, "Bayesian compressive sensing," *IEEE Trans. Signal Process.*, vol. 56, no. 6, pp. 2346–2356, June 2008.

[23] Q. Wu, Y. D. Zhang, M. G. Amin, and B. Himed, "Complex multitask Bayesian compressive sensing," in *Proc. IEEE Int. Conf. Acoust. Speech Signal Process.*, Florence, Italy, May 2014.

[24] Y. LeCun, Y. Bengio, and G. Hinton, "Deep learning," *Nature*, vol. 521, no. 7553, pp. 436–444, 2015.

[25] L. Zhang, F. Yang, Y. D. Zhang, and Y. J. Zhu, "Road crack detection with deep convolution neural network," in *Proc. IEEE Int. Conf. Image Process.*, Phoenix, AZ, Sept. 2016.